Illumination analysis of wave-equation imaging with "curvelets"

*Shen Wang *, Maarten V. de Hoop and Bjørn Ursin*

SUMMARY

We present a comprehensive framework for wave-equation illumination analysis and introduce a target-oriented illumination correction that simultaneously accounts for limited acquisition aperture and, locally, compensates for the so-called normal operator in inverse scattering to yield a "true-amplitude" image of reflectivity or reflection coefficient, while minimizing (orientation dependent) phase distortions and artifacts. To carry out the analysis we make use of "curvelets" (viewed as optimally localized plane waves) which provide the means of extracting directional information and hence form a natural candidate to generalize geophysical diffraction tomography.

INTRODUCTION

It remains a challenge to generate images that admit a quantitative interpretation in regions of complex geology, even if an accurate velocity or background model has been obtained. Typically, limited acquisition aperture gives rise to – dip dependent – image amplitude variations, and phase distortions and artifacts. Here, we develop a technique that addresses these illumination effects in the framework of wave-equation migration. Throughout we assume the single scattering approximation for reflection seismic data. The procedure contains elements of (regularized) Least-Squares migration (Kühl and Sacchi (2003); Clapp et al. (2005)), double focusing (and the notion of controlled illumination, see Rietveld and Berkhout (1994); Alai and Thorbecke (2008)), geophysical diffraction tomography (Devaney (1984); Wu and Toksöz (1987)), and is motivated by the illumination analysis of Xie et al. (2006) and Wu and Chen (2006).

We develop a relation between curvelet coefficients representing the image and the curvelet coefficients representing the (downward continued) data. The coefficients also immediately provide information about the directional dependence, that is, downward continued wave slowness vectors and image dips, and implicitly scattering angle (and azimuth). Indeed, the curvelet transform reveals the imprint of the ray geometry underlying the wave-equation illumination analysis which can be used as part of an imaging condition.

Andersson et al. (2008) derived and developed a multi-scale approach to wave propagation by solving a Volterra equation yielding the concentration of wave packets even in velocity models of limited smoothness. Building on this result, here, we develop the downward continuation counterpart of partial reconstruction based on the GRT (De Hoop et al. (2009)). Our point of departure is the unifying formulation for seismic inverse scattering by Stolk and De Hoop (2005, 2006). In our derivation we will point out analogies with the illumination analysis introduced by Luo et al. (2004); Xie et al. (2006); Wu and Chen (2006). We go beyond the latter analysis by connecting the data illumination with the normal operator both for generating images as well as common-image-point gathers.

Curvelets are different from "beamlets" (Chen et al. (2006)). Curvelets provide the harmonic analysis tool to sparsely represent the propagators (Smith (1998); Candès and Demanet (2005)) and localize the normal operator. In particular, one can obtain the inverse of the normal operator matrix via diagonal approximation (De Hoop et al. (2009)). The curvelet amplitude spectra are essentially window functions while curvelets themselves are well localized with decay tracing oriented ellipsoids. "Beamlets", on the other hand, are generated by windowed Fourier transforms.

We will begin with summarizing modeling of reflection seismic data in the Born approximation via extensions of the velocity contrast. we summarize directional (up/down) wavefield decomposition, introduce the double-square root (DSR) equation and discuss the associated thin-slab propagator. we derive the extended wave-equation imaging operator matrix adapted to contain an illumination correction, and then incorporate the compensation for the normal operator, within each thin slab, to arrive at the diffraction formulation of partial reconstruction.

THEORY

Following Stolk and De Hoop (2005), we write the Born approximation for single scattered waves in the form

$$\delta G(0,r,t,0,s) = \int_{\mathbb{R}^{n-1}\times\mathbb{R}_+} \int_{\mathbb{R}^{n-1}} \int_{-\infty}^{t} \int_{\mathbb{R}_+} G(0,r,t-t_0,z,x) \times \partial_{\bar{t}_0}^2 R(z,x,\bar{x},t_0-\bar{t}_0) G(z,\bar{x},\bar{t}_0,0,s)\, \mathrm{d}\bar{t}_0\, \mathrm{d}t_0\, \mathrm{d}\bar{x}\, \mathrm{d}x \mathrm{d}z, \quad (1)$$

where

$$R(z,x,\bar{x},t_0) = \delta(t_0)\delta(x-\bar{x})2\left(\frac{\delta c}{c_0^3}\right)\left(z,\frac{\bar{x}+x}{2}\right), \quad (2)$$

or

$$R = E_2E_1 2c_0^{-3}\delta c \quad (3)$$

represents the extension of velocity contrast. E_1 and E_2 are two extension operators. The scattering operator then follows to be

$$F:\ \delta c \mapsto LE_2E_1 2c_0^{-3}\delta c \quad (4)$$

it models deconvolved seismic reflection data, where the deconvolution includes ∂_t^{-2}. Accordingly, operator L will be defined as:

$$LR(s,r,t) = \int_{\mathbb{R}_+}\left\{\int_{\mathbb{R}^{n-1}}\int_{\mathbb{R}^{n-1}}\int_{\mathbb{R}}\left(\int_0^{t-t_0} G(0,r,t-t_0-\bar{t}_0,z,x) \times G(0,s,\bar{t}_0,z,\bar{x})\,\mathrm{d}\bar{t}_0\right) R(z,x,\bar{x},t_0)\,\mathrm{d}\bar{x}\,\mathrm{d}x\,\mathrm{d}t_0\right\}\mathrm{d}z. \quad (5)$$

Illumination analysis with "curvelets"

The double-square-root (DSR) propagator is given by

$$(H(z,z_0))(s,r,t,s_0,r_0,t_0) = \int_{\mathbb{R}} (G_-(z,z_0))(s,t-t_0-\bar{t}_0,s_0)(G_-(z,z_0))(r,\bar{t}_0,r_0)\,\mathrm{d}\bar{t}_0. \quad (6)$$

Here $(G_-(z,z_0))(r,\bar{t}_0,r_0,0)$ denotes the distribution kernel of $G_-(z,z_0)$, and $(H(z,z_0))(s,r,t,s_0,r_0,t_0)$ denotes the distribution kernel of $H(z,z_0)$ and is the Green's function of the DSR equation. Additionally, directional (up/down) decomposition of transient waves – in the "flux normalization" (see, for example, De Hoop (1996)) – is accomplished through the introduction of pseudodifferential operator, $Q_-(z,.) = Q_-(z,x,D_x,D_t)$, with so-called principal symbol,

$$\mathrm{i}\ \mathrm{sgn}(\omega)|\omega|^{-1/2}[c_0(z,x)^{-2} - \omega^{-2}\|\xi_x\|^2]^{-1/4}.$$

With this operator, the upward continuation analogue of (5) is given by (Stolk and De Hoop (2005))

$$LR := -\frac{1}{4} Q^*_{-,s}(0) Q^*_{-,r}(0) \int_{\mathbb{R}_+} H(0,z) Q_{-,s}(z) Q_{-,r}(z) R(z,.,.,.)\,\mathrm{d}z, \quad (7)$$

Furthermore, the DSR propagator can be approximated by a composition of thin-slab propagators (De Hoop et al. (2003); Le Rousseau (2006)); one such thin-slab propagator attains the form

$$(H(z'-\Delta,z'))(s,r,t,s',r',t') \approx (2\pi)^{-(2n-1)} \int\int\int \exp[\mathrm{i}(\langle \xi_s, s-s'\rangle + \langle \xi_r, r-r'\rangle - \Delta\Gamma(z',s,r,\xi_s,\xi_r,\omega))] \times \exp[\mathrm{i}\omega(t-t')]\,\mathrm{d}\xi_s \mathrm{d}\xi_r \mathrm{d}\omega. \quad (8)$$

This approximation has an error roughly of order $\Delta^{1/2}$.

METHODS

Here, we develop a description of the single scattering operator (cf. (4)) in terms of "curvelets", which leads to the matrix representations for the component operators, $Q_-(.)$ and L (cf. (7)) while making use of (8).

Decomposition of the scattering operator into curvelets

Through composition (4), we build up the action of F on a curvelet. The frame of curvelets, $\{\varphi_\gamma\}$ is introduced in Appendix. We consider $2c_0^{-3}\delta c = \varphi_{\gamma_0}$, with $\gamma_0 = ((z_{j0},x_{j0}),\nu_0,k_0)$, which we can think of as being approximately supported on an oriented ellipsoid, centered at (z_{j0},x_{j0}) in space and $(\xi_z,\xi_x) = 2^{k_0}\nu_0$ in wavenumber; ν_0 can be thought of as a dip. The points (z_{j0},x_{j0}) lie on a tilted lattice; see Fig. 1.

Then after applying operator F in (4) to such single curvelet with the method of stationary phase, and let the matrix for the (invertible) propagator $H(0,z_{m-1})$ be denoted by $[H(0,z_{m-1})]$, let $[Q^*_{-,s}(0)Q^*_{-,r}(0)]$ denote the matrix associated with pseudodifferential operator $Q^*_{-,s}(0)Q^*_{-,r}(0)$, we find that the matrix

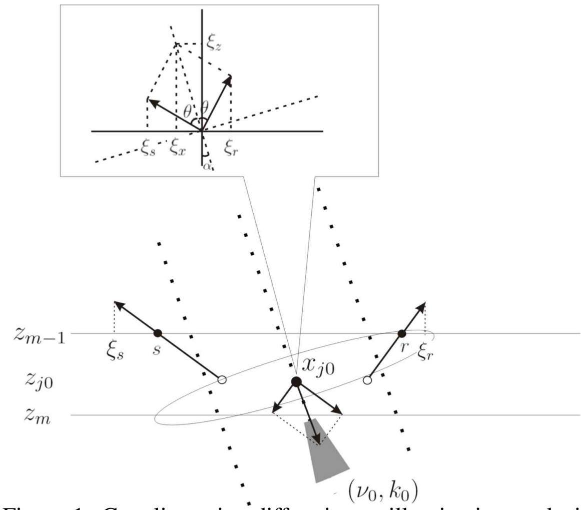

Figure 1: Coupling microdiffraction to illumination analysis: Dipping contrast curvelet (indicated by the ellipse), source and receiver wave vectors, lattice of translations and thin slab.

elements of F attain the form

$$\langle \psi_\gamma, F\varphi_{\gamma_0}\rangle_{(s,r,t)} = -\frac{1}{4}\sum_{\gamma''}[Q^*_{-,s}(0)Q^*_{-,r}(0)]_{\gamma\gamma''}\sum_{m=1}^{\infty}\sum_{\gamma'}[H(0,z_{m-1})]_{\gamma''\gamma'}V_{\gamma';\gamma_0}(z_{m-1}). \quad (9)$$

where

$$V_{\gamma_0}(z_{m-1},s,r,t) \approx (2\pi)^{-(2n-1)}\int\int\int Q_{-,s}(z_{j0},s,\xi_s,\omega) \times Q_{-,r}(z_{j0},r,\xi_r,\omega)\,\hat{\varphi}_{\nu_0,k_0}(\Gamma(z_m,s,r,\xi_s,\xi_r,\omega),\xi_s+\xi_r) \times \exp[-\mathrm{i}(z_{j0}-z_{m-1})\Gamma(z_m,s,r,\xi_s,\xi_r,\omega)] \times \exp[\mathrm{i}(\langle\xi_s,s-x_{j0}\rangle + \langle\xi_r,r-x_{j0}\rangle + \omega t)]\,\mathrm{d}\xi_s\mathrm{d}\xi_r\mathrm{d}\omega, \quad (10)$$

which is viewed as a mapping of the contrast curvelet, φ_{γ_0}, to virtual subsurface reflection data, $V_{\gamma_0}(z_{m-1},.,.,.)$, provided that $z_{j0}\in(z_{m-1},z_m)$ – we assume that the z_{j0} do not coincide with z_m, $m = 0,1,2,\ldots$; see Fig. 1. We expand $V_{\gamma_0}(z_{m-1},.,.,.)$ into curvelets, that is,

$$V_{\gamma_0}(z_{m-1},.,.,.) = \sum_{\gamma'} V_{\gamma';\gamma_0}(z_{m-1})\varphi_{\gamma'} \quad (11)$$

$$V_{\gamma';\gamma_0}(z_{m-1}) = \langle\psi_{\gamma'}, V_{\gamma_0}(z_{m-1},.,.,.)\rangle_{(s,r,t)} \quad (12)$$

Migration and micro-diffraction tomography

Here, we describe imaging in the downward continuation approach in terms of "curvelets". We decompose the surface reflection data, $d = \sum_\gamma d_\gamma\psi_\gamma$; we write d for the sequence of coefficients d_γ. We let the adjoint, F^*, of F, act on a data curvelet, ψ_γ,

$$F^*\psi_\gamma(z,.) = R_1R_2Q^*_{-,s}(z)Q^*_{-,r}(z) \sum_{\tilde{\gamma}',\tilde{\gamma}''} H(z_{\tilde{m}-1},z)^*\psi_{\tilde{\gamma}'}\,[H(0,z_{\tilde{m}-1})^*]_{\tilde{\gamma}'\tilde{\gamma}''}[Q_{-,s}(0)Q_{-,r}(0)]_{\tilde{\gamma}''\gamma}\left(-\frac{1}{4}\right), \quad (13)$$

if $z \in [z_{\bar{m}-1}, z_{\bar{m}})$; here, $R_1 = E_1^*$ and $R_2 = E_2^*$ are restrictions representing the traditional imaging conditions setting time (R_2) and subsurface offset (R_1) to zero. If curvelet components, d_γ, with index γ in the set $\mathscr{S}$ can be observed at the surface ($\mathscr{S}$ is derived from the acquisition geometry), the associated subsurface illumination is captured in the matrix

$$
\begin{aligned}
&[A^{\mathscr{S}}(z_{\bar{m}-1}, z_{m-1})]_{\tilde{\gamma}'\gamma} = \\
&\quad \sum_{\tilde{\gamma}'',\gamma,\tilde{\gamma},\gamma''} [H(0, z_{\bar{m}-1})^*]_{\tilde{\gamma}'\tilde{\gamma}''}[Q_{-,s}(0)Q_{-,r}(0)]_{\tilde{\gamma}''\gamma} \\
&\qquad \times \Pi^{\mathscr{S}}_{\gamma\tilde{\gamma}}\, [Q^*_{-,s}(0)Q^*_{-,r}(0)]_{\tilde{\gamma}\gamma''}[H(0, z_{m-1})]_{\gamma''\gamma'} \qquad (14)
\end{aligned}
$$

with $\Pi^{\mathscr{S}} = \Pi\, \mathbf{1}^{\mathscr{S}}$, which can be loosely thought of as a projection onto $\mathscr{S}$; for the introduction of Π, see Appendix A. The inverse diagonal approximation of $[A^{\mathscr{S}}(z_{m-1}, z_{m-1})]$ is given by

$$
\widetilde{D}_{\gamma'}(z_{m-1})^{-1} = [A^{\mathscr{S}}(z_{m-1}, z_{m-1})]^{-1}_{\gamma'\gamma'}\Pi_{\gamma'\gamma'};
$$

this approximation reflects the inverse of $[A^{\mathscr{S}}(z_{m-1}, z_{m-1})]$ up to an error of order $2^{-k/2}$ (De Hoop et al. (2009)).

Reconstruction

Here, we analyze the relationship between the illumination-corrected image and the contrast. We arrive at a normal operator for "micro"-diffraction tomography: The illumination-corrected image corresponds with $\widetilde{N}'\, 2c_0^{-3}\delta c$. Here, $\widetilde{N}' = (F^*)'\mathrm{C}^{-1}\Pi^{\mathscr{S}}\mathrm{C}F$, where C denotes the curvelet transform, with matrix representation

$$
\begin{aligned}
[\widetilde{N}']_{\gamma_0\gamma_0} = \left(-\frac{1}{4}\right)^2 \sum_{\bar{m},m=1}^{\infty} \sum_{\tilde{\gamma}',\gamma'} V^*_{\gamma_0;\tilde{\gamma}'}(z_{\bar{m}-1})\widetilde{D}_{\tilde{\gamma}'}(z_{\bar{m}-1})^{-1} \\
\times [A^{\mathscr{S}}(z_{\bar{m}-1}, z_{m-1})]_{\tilde{\gamma}'\gamma'} V_{\gamma';\gamma_0}(z_{m-1}). \qquad (15)
\end{aligned}
$$

Because $\widetilde{N}'$ is a pseudodifferential operator, its corresponding matrix $[\widetilde{N}']$ is diagonally dominant, while

$$
\begin{aligned}
[\widetilde{N}']_{\gamma_0\gamma_0} \approx \left(-\frac{1}{4}\right)^2 \sum_{\tilde{\gamma}',\gamma'} V^*_{\gamma_0;\tilde{\gamma}'}(z_{m_0-1})\widetilde{D}_{\tilde{\gamma}'}(z_{m_0-1})^{-1} \\
\times [A^{\mathscr{S}}(z_{m_0-1}, z_{m_0-1})]_{\tilde{\gamma}'\gamma'} V_{\gamma';\gamma_0}(z_{m_0-1}) \qquad (16)
\end{aligned}
$$

with $[z_{m_0-1}, z_{m_0}) \ni z_{j0}$ as before.

We set up the normal equations for the extended contrast h, which we subject to the decomposition, $h = \sum_{\gamma_0} h_{\gamma_0}\varphi_{\gamma_0}$. Thus, we redefine (cf. (12))

$$
V_{\gamma';\gamma_0}(z_{m_0-1}) := [K_{m_0-1}]_{\gamma'\gamma_0}, \qquad (17)
$$

with

$$
K_{m-1}\ :\ h \rightarrow \int_{z_{m-1}}^{z_m} H(z_{m-1}, z')Q_{-,s}(z')Q_{-,r}(z')E_2 h(z', .,.)\, \mathrm{d}z',
$$

the propagation of singularities of which is described by a transformation, $\Sigma_{K;m-1}$ say, obtained by ray tracing.

We solve the normal equations in two steps. First, we consider subsurface data coefficients $d_{\gamma'}(z_{m_0-1})$ and carry out a "partial" redatuming by solving

$$
\begin{aligned}
&\sum_{\gamma'} \widetilde{D}_{\tilde{\gamma}}(z_{m_0-1})^{-1}[A^{\mathscr{S}}(z_{m_0-1}, z_{m_0-1})]_{\tilde{\gamma}\gamma'} d_{\gamma'}(z_{m_0-1}) \\
&= \sum_{\tilde{\gamma}'',\gamma,\tilde{\gamma}} \widetilde{D}_{\tilde{\gamma}}(z_{m_0-1})^{-1}[H(0, z_{m_0-1})^*]_{\tilde{\gamma}\tilde{\gamma}''}[Q_{-,s}(0)Q_{-,r}(0)]_{\tilde{\gamma}''\gamma} \\
&\qquad\qquad \times \left(-\frac{1}{4}\right)\Pi^{\mathscr{S}}_{\gamma\tilde{\gamma}} d_{\tilde{\gamma}}, \qquad (18)
\end{aligned}
$$

The second step concerns a micro-diffraction problem. We carry out the "partial" reconstruction by solving

$$
\begin{aligned}
&\widetilde{D}_{\Xi}(z_{m_0-1})^{-1}[K^*_{m_0-1}]\Pi^{\mathscr{S}(z_{m_0-1})}[K_{m_0-1}]\Pi^{\mathscr{C}(z_{m_0-1})}(h) \\
&\qquad = \widetilde{D}_{\Xi}(z_{m_0-1})^{-1}[K^*_{m_0-1}]\Pi^{\mathscr{S}(z_{m_0-1})}(d(z_{m_0-1})) \qquad (19)
\end{aligned}
$$

for (h) upon substituting for $(d(z_{m_0-1}))$ the solution of (18).

EXAMPLES

The common component in the diffraction and reflection formulation for illumination analysis is the correction with $\widetilde{D}_{\gamma'}(z_{m-1})$. We illustrate this diagonal matrix by computing $\sum_{\tilde{\gamma}}[A^{\mathscr{S}}(z_{\bar{m}-1}, z_{m-1})]_{\tilde{\gamma}\gamma}\psi_{\tilde{\gamma}}$, in particular at $\bar{m} = m$, and assessing how well the underlying matrix is approximated by its diagonal.

As the background (c_0) we use the low velocity lens model depicted in Fig. 2; the dot in this figure indicates the scattering point position, (z, x), common in the subsequent numerical examples, and the dashed line indicates the chosen value of z_{m-1}. The lens is responsible for the formation of caustics. The local reflector dips $((\xi_z, \xi_x)/\|(\xi_z, \xi_x)\|)$ and scattering angles (corresponding with p) considered are indicated by the arrow patterns inside the three boxes at the bottom; we let $k_0 = 1$. We begin with generating the $\varphi_{\gamma'}$'s at depth z_{m-1}

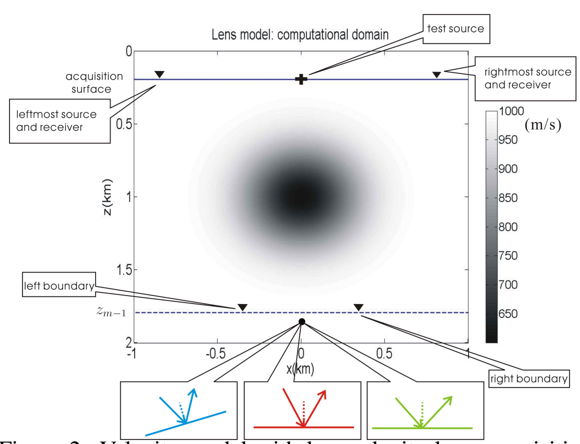

Figure 2: Velocity model with low-velocity lens, acquisition surface and illumination depth, z_{m-1}. Three cases with various scattering and dip angles are considered

indicated by the dashed line in Fig. 2, locally, for subsurface sources and receivers in the between the solid triangles; they are plotted in Figs. 3(a) (top), 3(b) (top) and 3(c) (top). We then compute $\sum_{\tilde{\gamma}'} [A^{\mathscr{S}}(z_{\tilde{m}-1}, z_{m-1})]_{\tilde{\gamma}'\gamma'} \psi_{\tilde{\gamma}'}$, where $\mathscr{S}$ is implied by the limited acquisition geometry indicated by the solid triangles on the acquisition surface in Fig. 2. The results, representing our illumination analysis, are illustrated in Figs. 3(a) (bottom), 3(b) (bottom) and 3(c) (bottom). We also computed $\sum_{\tilde{\gamma},\gamma''} [Q^*_{-,s}(0)Q^*_{-,r}(0)]_{\tilde{\gamma}\gamma''}[H(0,z_{m-1})]_{\gamma''\gamma}\varphi_{\tilde{\gamma}}$ for a test source location (indicated by a $+$ in Fig. 2), see Fig. 3(d). We observe the expected localization property (from subsurface to surface) of curvelets in phase space; for comparison, we also simulated the full synthetic data for the zero dip case (top left).

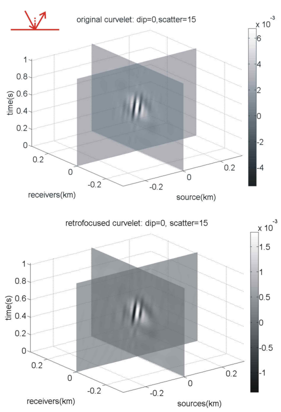

(a)

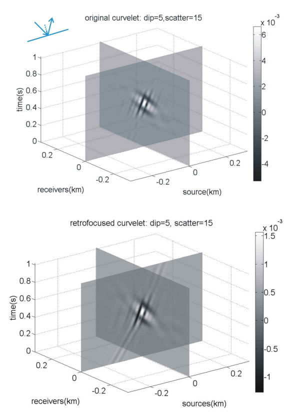

(b)

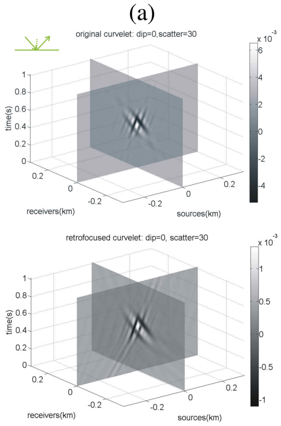

(c)

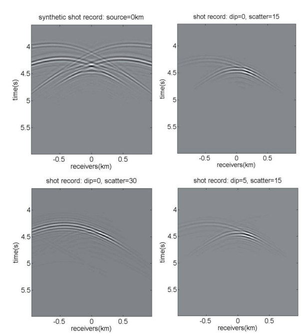

(d)

Figure 3: $(a)(b)(c)$ Original subsurface data curvelet (top) and retrofocused subsurface data (bottom). (d) surface data generated in the model and by upward continuing the subsurface data curvelet in $(a)(b)(c)$. We note the localization of these three surface data

Finally, we visualize the decay of $[A^{\mathscr{S}}(z_{m-1}, z_{m-1})]_{\tilde{\gamma}'\gamma'}$ away from its diagonal. We take the value of γ' corresponding with the curvelet in Fig. 3 (top). In Fig. 4 we plot, at scale $k' = 2$, the values of $|[A^{\mathscr{S}}(z_{m-1}, z_{m-1})]_{\tilde{\gamma}'\gamma'}|$ if $\tilde{\gamma}'$ differs from γ' by translations $((s,r,t)_{\tilde{j}'} \neq (s,r,t)_{j'})$ or rotations $(\bar{\nu}' \neq \nu')$. This provides a quantification of accuracy implying whether iterations are needed for the illumination correction beyond the inverse diagonal approximation.

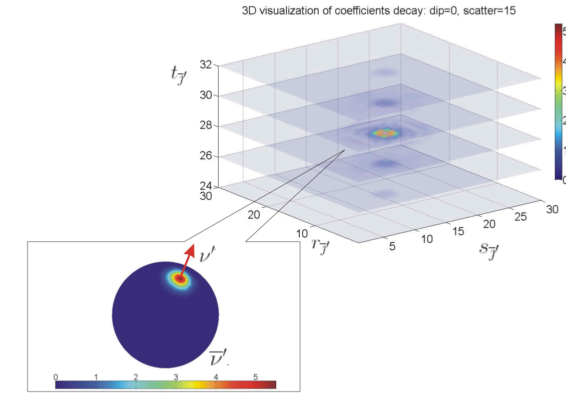

Figure 4: Visualization of the decay of $[A^{\mathscr{S}}(z_{m-1}, z_{m-1})]_{\tilde{\gamma}'\gamma'}$ away from its diagonal. Here, the value of γ' corresponds with the curvelet in Fig. 3(a). The values of $|[A^{\mathscr{S}}(z_{m-1}, z_{m-1})]_{\tilde{\gamma}'\gamma'}|$ are plotted if $\tilde{\gamma}'$ differs from γ' by translations $((s,r,t)_{\tilde{j}'} \neq (s,r,t)_{j'})$ or rotations $(\bar{\nu}' \neq \nu')$.

CONCLUSIONS

We have developed a technique to compensate for illumination effects in the framework of wave-equation migration. We constructed amplitude "correction" that account for limited acquisition aperture (illumination) and that compensate for the so-called normal operator to yield a "true-amplitude" image of reflectivity or local reflection coefficient, while minimizing distortions and artifacts. We establish a relationship with geophysical diffraction tomography in terms of curvelets. We decompose the subsurface into thin slabs. The normal operator correction pertains to diffraction or reflection within the thin slabs, while the illumination correction pertains to downward continuation to the tops of the thin slabs.

APPENDIX: WAVE PACKETS AND CURVELETS

We introduce boxes (along the ξ_1-axis, that is, $\xi' = \xi_1$)

$$B_k = \left[\xi'_k - \frac{L'_k}{2}, \xi'_k + \frac{L'_k}{2}\right] \times \left[-\frac{L''_k}{2}, \frac{L''_k}{2}\right]^{m-1},$$

where the centers ξ'_k, as well as the side lengths L'_k and L''_k, satisfy the parabolic scaling condition. In the (co-)frame construction, we have two sequences of smooth functions, $\hat{\chi}_{\nu,k}$ and $\hat{\beta}_{\nu,k}$, which form a co-partition of unity

$$\hat{\chi}_0(\xi)\hat{\beta}_0(\xi) + \sum_{k\geq 1}\sum_{\nu} \hat{\chi}_{\nu,k}(\xi)\hat{\beta}_{\nu,k}(\xi) = 1, \qquad (20)$$

The frame elements ($k \geq 1$) are then defined in the Fourier domain as

$$\hat{\varphi}_\gamma(\xi) = \rho_k^{-1/2}\hat{\chi}_{\nu,k}(\xi)\exp[-\mathrm{i}\langle x_j, \xi\rangle], \quad \gamma = (x_j, \nu, k), \quad (21)$$

and similarly for $\hat{\psi}_\gamma(\xi)$. We obtain the transform pair

$$v_\gamma = \int v(x)\overline{\psi_\gamma(x)}\,\mathrm{d}x, \qquad v(x) = \sum_\gamma v_\gamma \varphi_\gamma(x) \qquad (22)$$

EDITED REFERENCES

Note: This reference list is a copy-edited version of the reference list submitted by the author. Reference lists for the 2009 SEG Technical Program Expanded Abstracts have been copy edited so that references provided with the online metadata for each paper will achieve a high degree of linking to cited sources that appear on the Web.

REFERENCES

Alai, R., and J. Thorbecke, 2008, Illumination of the subsurface towards identifying shadow zones and optimizing target images: 78th Annual International Meeting, SEG, Expanded Abstracts, 193–197.

Andersson, F., M. Carlsson, and M. V. de Hoop, 2008, Nonlinear approximation of functions by sums of wave packets: Applied and Computational Harmonic Analysis, submitted.

Andersson, F., M. V. de Hoop, H. F. Smith, and G. Uhlmann, 2008, A multi-scale approach to hyperbolic evolution equations with limited smoothness: Communications in Partial Differential Equations, **33**, 988–1017.

Ayzenberg, M. A., A. M. Aizenberg, H. B. Helle, K. D. Klem-Musatov, J. Pajchel, and B. Ursin, 2007, 3D diffraction modelling of singly scattered acoustic wavefields based on the combination of surface integral propagators and transmission operators: Geophysics, **72**, no. 5, SM19–SM34.

Bear, G., C. Liu, R. Lu, and D. Willen, 2000, The construction of subsurface illumination and amplitude maps via ray tracing: The Leading Edge, **19**, 726–728.

Brytik, V., M. V. de Hoop, and M. Salo, 2008, Sensitivity analysis of wave-equation tomography: A multi-scale approach: Journal of Fourier Analysis and Applications, submitted.

Candés, E. J., and L. Demanet, 2005, The curvelet representation of wave propagators is optimally sparse: Communications on Pure and Applied Mathematics, **58**, 1472–1528.

Candés, E. J., L. Demanet, L., D. Donoho, and L. Ying, 2006, Fast discrete curvelet transforms: SIAM Multiscale Modeling Simulation, **5-3**, 861–899.

Candés, E. J., and D. Donoho, 2004, New tight frames of curvelets and optimal representations of objects with piecewise C. 2 singularities: Communications on Pure and Applied Mathematics, **57**, 219–266.

———, 2005, Continuous curvelet transform: I. Resolution of the wavefront set: Applied and Computational Harmonic Analysis, **19**, 162–197.

———, 2005, Continuous curvelet transform: II. Discretization and frames: Applied and Computational Harmonic Analysis, **19**, 198–222.

Chauris, H., and T. Nguyen, 2008, Seismic demigration/migration in the curvelet domain: Geophysics, **73**, no. 2, S35–S46.

Chen, L., R.-S. Wu, and Y. Chen, 2006, Beamlet migration based on Gabor-Daubechies frame decomposition: Geophysics, **71**, no. 2, S37–S52.

Clapp, M. L., R. G. Clapp, and B. Biondi, 2005, Regularized least-squares inversion for 3-D subsalt imaging: 75th Annual International Meeting, SEG, Expanded Abstracts, 1814–1817.

De Bruin, C. G. M., C. P. A. Wapenaar, and A. J. Berkhout, 1990, Angle-dependent reflectivity by means of prestack migration: Geophysics, **55**, 1223–1234.

de Hoop, M. V., 1996, Generalization of the Bremmer coupling series: Journal of Mathematical Physics, **37**, 3246–3282.

de Hoop, M. V., J. H. Le Rousseau, and B. L. Biondi, 2003, Symplectic structure of wave-equation imaging: A path-integral approach based on the double-square-root equation: Geophysical Journal International, 153, 52–74.

de Hoop, M. V., J. H. Le Rousseau, and R.-S. Wu, 2000, Generalization of the phase-screen approximation for the scattering of acoustic waves: Wave Motion, **31**, 43–70.

de Hoop, M. V., H. F. Smith, G. Uhlmann, and R. D. Van der Hilst, 2009, Seismic imaging with the generalized Radon transform: A curvelet transform perspective: Inverse Problems, **25**, doi:10.1088/0266-5611/25/2/025005.

de Hoop, M. V., C. Spencer, and R. Burridge, 1999, The resolving power of seismic amplitude data: An anisotropic inversion/migration approach: Geophysics, **64**, 852–873.

Devaney, A. J., 1984, Geophysical diffraction tomography: IEEE Transactions on Geoscience and Remote Sensing, GE-22, 3–13.

Douma, H., and M. V. de Hoop, 2007, Leading-order seismic imaging using curvelets: Geophysics, **72**, no. 6, S231–S248.

Duchkov, A. A., F. Andersson, and M. V. de Hoop, 2008, Discrete, almost symmetric wave packets and multi-scale geometric representation of (seismic) waves: Journal of Computational Physics, submitted.

Duchkov, A. A., M. V. de Hoop, and A. S. Sá Barreto, 2008, Evolution-equation approach to seismic image, and data, continuation: Wave Motion, **45**, 952–969.

Gelius, L. J., I. Lecomte, and H. Tabti, 2002, Analysis of the resolution function in seismic prestack depth imaging: Geophysical Prospecting, **50**, 505–515.

Kuhl, H., and M. D. Sacchi, 2003, Least-squares wave-equation migration for AVP/AVA inversion: Geophysics, **68**, 262–273.

Le Rousseau, J. H., 2006, Fourier-integral-operator approximation of solutions to first-order hyperbolic pseudodifferential equations I: Convergence in Sobolev spaces: Communications in Partial Differential Equations, **31**, 867–906.

Li, C.-F., and Liner, C. L., 2008, Wavelet-based detection of singularities in acoustic impedance from surface reflection data: Geophysics, **73**, no. 1, V1–V9.

Luo, M., J. Cao, X.-B. Xie, and R.-S. Wu, 2004, Comparison of illumination analyses using one-way and full-wave propagators: 74th Annual International Meeting, SEG, Expanded Abstracts, 67–70.

Muerdter, D., M. Kelly, and D. Ratcliff, 2001, Understanding subsalt illumination through ray-trace modeling, Part 2: Dipping salt bodies, salt peaks, and nonreciprocity of subsalt amplitude response: The Leading Edge, **20**, 688–697.

Muerdter, D., and D. Ratcliff, 2001, Understanding subsalt illumination through ray-trace modeling, Part 1: Simple 2-D salt models: The Leading Edge, **20**, 578–594.

———, 2001, Understanding subsalt illumination through ray-trace modeling, Part 3: Salt ridges and furrows, and the impact of acquisition orientation: The Leading Edge, **20**, 803–816.

Rickett, J. E., 2003, Illumination-based normalization for wave-equation depth migration: Geophysics, **68**, 1371–1379.

Rietveld, W. E. A., and A. J. Berkhout, 1994, Prestack depth migration by means of controlled illumination: Geophysics, **59**, 801–809.

Smith, H. F., 1998, A parametrix construction for wave equations with C. 1,1 coefficients: Annales de l'Institute Fourier, **48**, 797–835.

Stolk, C. C., 2004, A pseudodifferential equation with damping for one-way wave propagation in inhomogeneous acoustic media: Wave Motion, 40, no. 2, 111–121.

Stolk, C. C., and M. V. de Hoop, 2002, Microlocal analysis of seismic inverse scattering in anisotropic elastic media: Communications on Pure and Applied Mathematics, 55, 261–301.

———, 2005, Modeling of seismic data in the downward continuation approach: SIAM Journal on Applied Mathematics, **65**, 1388–1406.

———, 2006, Seismic inverse scattering in the downward continuation approach: Wave Motion, **43**, 579–598.

Symes, W.W., 2008, Approximate linearized inversion by optimal scaling of prestack depth migration: Geophysics, **73**, no. 2, R23–R35.

Xie, X.-B., S. Jin, and R.-S. Wu, 2006, Wave-equation-based seismic illumination analysis: Geophysics, **71**, no. 5, S169–S177.

Wapenaar, C. P. A., 1998, Seismic reflection and transmission coefficients of a self-similar interface: Geophysical Journal International, **135**, 585–594.

Wu, R.-S., and L. Chen, 2006, Directional illumination analysis using beamlet decomposition and propagation: Geophysics, **71**, no. 4, S147–S159.

Wu, R.-S., and M. N. Toksöz, 1987, Diffraction tomography and multisource holography applied to seismic imaging: Geophysics, **52**, 11–25.